Classical–quantum correspondence for non-Hermitian quantum dynamics

Eva-Maria Graefe[1,2], **Matthias Strauß**[1] **and Hans Jürgen Korsch**[1]

[1] FB Physik, TU Kaiserslautern, D–67653 Kaiserslautern, Germany
[2] Department of Mathematics, Imperial College London, London, SW7 2AZ, United Kingdom

E-mail: korsch@physik.uni-kl.de

Abstract. xxx

PACS numbers: 03.65.-w, 03.65Sq, 45.20-d

Submitted to: *J. Phys. A: Math. Gen.*

1. Introduction

[1] [2,3]

Here we will study the dynamics generated by a non-Hermitian Hamiltonian

$$\hat{H} = \hat{H} - \mathrm{i}\hat{\Gamma} \tag{1}$$

with $\hat{H} = \hat{H}^\dagger$ and a non-negative damping term $\hat{\Gamma} = \hat{\Gamma}^\dagger$ in comparison with its classical counterpart derived in [1]. If the Hamiltonian is time independent, the dynamics can be treated easily in terms of the non-Hermitian eigenstates of $\hat{H}$ with eigenvalues $E_n = E_n - \mathrm{i}\Gamma_n$, $n = 0, 1, \ldots$ as described in [1], where the eigenstates are ordered according to their decay rate, i.e. as $\Gamma_n \leq \Gamma_{n+1}$. In the long time limit all states approach the most stable eigenstate $n = 0$. If the Hamiltonian depends periodically on time, the system can be treated in a similar way in terms of Floquet states.

Note that, while the norm $n = \langle\psi|\psi\rangle$ decays to zero, the expectation value of an operator $\hat{A}$,

$$\langle\hat{A}\rangle = \frac{\langle\psi|\hat{A}|\psi\rangle}{\langle\psi|\psi\rangle}, \tag{2}$$

typically remains finite.

In [1] the classical limit of such a non-Hermitian quantum system was discussed and applied to a few examples, namely the celebrated damped and driven harmonic oscillator, an anharmonic oscillator and an angular momentum system. Here we will study this approximation in more detail and present more examples for systems which can be written in terms of bosonic creation and annihilation operators $\hat{a}$ and $\hat{a}^\dagger$ with commutator $[\hat{a}, \hat{a}^\dagger] = 1$. For simplicity we use units with $\hbar = 1$ in the following.

Basically, the classical approximation assumes that an initially coherent state remains coherent. This is guaranteed if the the Hamiltonian is linear in the generators $\hat{a}$, $\hat{a}^\dagger$ and

$\hat{a}^\dagger\hat{a}+1/2$ of the harmonic oscillator algebra, but otherwise only approximate. Then one can show that the $\alpha=\langle\hat{a}\rangle$ and $\alpha^*=\langle\hat{a}^\dagger\rangle$ satisfy the equations of motion

$$\mathrm{i}\frac{\mathrm{d}\alpha}{\mathrm{d}t}=\frac{\partial H}{\partial\alpha^*}=\frac{\partial H}{\partial\alpha^*}-\mathrm{i}\frac{\partial\Gamma}{\partial\alpha^*},\qquad \mathrm{i}\frac{\mathrm{d}\alpha^*}{\mathrm{d}t}=-\frac{\partial H^*}{\partial\alpha}=-\frac{\partial H}{\partial\alpha}-\mathrm{i}\frac{\partial\Gamma}{\partial\alpha}, \tag{3}$$

where $H(\alpha,\alpha^*)$ and $\Gamma(\alpha,\alpha^*)$ are the (normally ordered) operators $\hat{H}(\hat{a},\hat{a}^\dagger)$ and $\hat{\Gamma}(\hat{a},\hat{a}^\dagger)$ where $\hat{a}$ and $\hat{a}^\dagger$ are replaced by α and α^*, respectively. In addition, the norm n decays as

$$\hbar\dot{n}=-2\big(\Gamma(\alpha,\alpha^*)+\Gamma_0\big)n \tag{4}$$

where the constant Γ_0 accounts for the finite decay rate in the long time limit.

Rewritten in terms of the position and momentum variables

$$q=\big(\alpha^*+\alpha\big)/\sqrt{2}\,,\quad p=\mathrm{i}\big(\alpha^*-\alpha\big)/\sqrt{2} \tag{5}$$

the equations of motion are

$$\dot{q}=\frac{\partial H}{\partial p}-\frac{\partial\Gamma}{\partial q}\quad\text{and}\quad \dot{p}=-\frac{\partial H}{\partial q}-\frac{\partial\Gamma}{\partial p}. \tag{6}$$

If these generalized canonical equations are expressed as a vector field on phase space $\vec{x}=(q,p)^T$ with $\vec{F}=\big(\partial_q H-\partial_q\Gamma,-\partial_p H-\partial_p\Gamma\big)^T$

$$\dot{\vec{x}}=\vec{F}(\vec{x}) \tag{7}$$

we find

$$\mathrm{div}\,\vec{F}=\partial_q F_q+\partial_p F_p=-\partial^2_{qq}\Gamma-\partial^2_{pp}\Gamma=-\Delta\Gamma\,, \tag{8}$$

i.e. the phase space volume δV shrinks with a rate proportional to the Laplacian of the damping function Γ:

$$\frac{1}{\delta V}\frac{\mathrm{d}\,\delta V}{\mathrm{d}t}=\mathrm{div}\,\vec{F}=-\Delta\Gamma\,. \tag{9}$$

For the time evolution of a dynamical variable $A(q,p,t)$ we find in an abbreviated notation

$$\dot{A}=\{A,\,H\}-\{\,A,\,\Gamma\}_+ +\partial_t A \tag{10}$$

with the Poisson bracket $\{A,\,B\}=\partial_q A\partial_p B-\partial_p A\partial_q B$ and $\{A,\,B\}_+=\partial_q A\partial_q B+\partial_p A\partial_p B$.

Eva: dein neues paper einbauen: [4]

2. A damped nonlinear oscillator

The nonlinear oscillator

$$\hat{H}=\Delta\omega\,\hat{a}^\dagger\hat{a}+\beta(\hat{a}^\dagger+\hat{a})+\chi(\hat{a}^\dagger\hat{a})^2 \tag{11}$$

is studied by many groups in different context (see, e.g., [5–7] and references therein xxx check more recent work). Here we follow the notation of [7] where the parameter $\Delta\omega$ is denoted as a 'detuning'.

In [5–7] the oscillator (11) is damped by coupling to a bath and the quantum dynamics is studied in terms of a density matrix evolution where the system-bath coupling is described in a Lindblad form or by quantum state diffusion. xxx check [5] Here we describe damping by an effective non-hermitian Hamiltonian (1) with

$$\hat{\Gamma}=\frac{\kappa}{2}\big(\hat{a}^\dagger\hat{a}+1/2\big)\,,\quad \kappa>0 \tag{12}$$

as motivated in [1]. For this oscillator, the classical Hamiltonian H and damping Γ are given by

$$H(\alpha,\alpha^*) = (\Delta\omega+\chi)\alpha^*\alpha+\beta(\alpha^*+\alpha)+\chi\alpha^{*2}\alpha^2\,, \quad \Gamma(\alpha,\alpha^*) = \frac{\kappa}{2}\alpha^*\alpha \tag{13}$$

and the corresponding equation of motion (3) is

$$\mathrm{i}\frac{\mathrm{d}\alpha}{\mathrm{d}t} = -\mathrm{i}\big(\beta+(\Delta\omega+\chi)\alpha+2\chi\alpha^2\alpha^*\big)-\frac{\kappa}{2}\alpha\,. \tag{14}$$

Note that this classical generalized canonical equation precisely agrees with the classical limit derived in [5,7], however for a different quantum system.

In terms of position and momentum variables the equations transform into

$$H(p,q) = \frac{\Delta\omega+\chi}{2}\left(p^2+q^2\right)+\beta\sqrt{2}q+\frac{\chi}{4}\left(p^2+q^2\right)^2\,, \quad \Gamma(p,q) = \frac{\kappa}{4}\left(p^2+q^2+2\right) \tag{15}$$

and

$$\dot{q} = (\Delta\omega+\chi)p-\frac{\kappa}{2}q+\chi(p^2+q^2)p \tag{16}$$

$$\dot{p} = -\beta\sqrt{2}-(\Delta\omega+\chi)q-\frac{\kappa}{2}p-\chi(p^2+q^2)q\,. \tag{17}$$

Let us first discuss in some detail the classical phase space dynamics. First we observe from (9) and (15) that the divergence of the phase space vector field is equal to $-\kappa<0$, i.e. the volume element in phase space is shrinking with a constant rate.

As already stated in [7], the stationary points can be obtained form the solutions of

$$|\alpha|^2\left(\kappa^2/4+(\Delta\omega+\chi+2\chi|\alpha|^2)^2\right)-\beta^2 = 0\,. \tag{18}$$

This third-order polynomial in $|\alpha|^2$ with real coefficients possesses one or three real valued solutions. For such a solution the real and imaginary parts of the fixed point α, i.e. the values of q and p, are given by

$$\frac{\mathrm{Re}\,\alpha}{|\alpha|^2} = -\frac{\Delta\omega+\chi+2\chi|\alpha|^2}{\beta}\,, \quad \frac{\mathrm{Im}\,\alpha}{|\alpha|^2} = -\frac{\kappa}{2\beta} \tag{19}$$

(note that the wrong sign in the real part in the formula given in [7]). There exists a regime, where there are three fixed points, namely two stable sinks and one unstable saddle point. In the monostable regime, we have a single sink attracting the whole phase space. The conditions for the parameters defining this bistable regime can be found in equation (9) in [7].

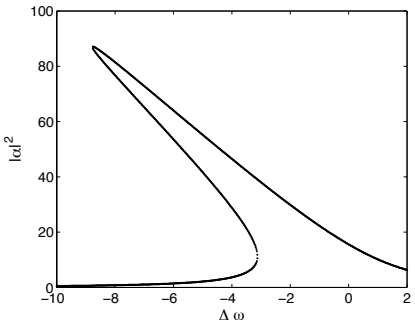

Figure 1. Classical fixed points $|\alpha|^2$ as a function of $\Delta\omega$ for $\kappa = 1.5$, $\beta = -7$ and $\chi = 0.05$. Compare figure 1 in [7].

As an example, figure 1 shows the real valued solutions of (18) for $\kappa = 1.5$, $\beta = -7$ and $\chi = 0.05$ as a function of $\Delta\omega$ (also shown in figure 1 in [7]). In the region with three solutions, the upper and lower branches are stable and the one in the middle is unstable. Figure 2 shows the phase space flow for $\Delta\omega = -5$, i.e. in the bistable region. One can clearly see the two stable fixed points, the sinks, at $(q_1, p_1) = (-2.04, 0.32)$ and $(q_2, p_2) = (6.36, 8.36)$ and an unstable one, a saddle point at $(q_3, p_3) = (-6.59, 6.31)$.

The classical phase space is organized by the stable and unstable manifolds of the saddle point, the separatrices, which are shown in figure 3. The stable manifolds separate the basins of attraction of the two sinks.

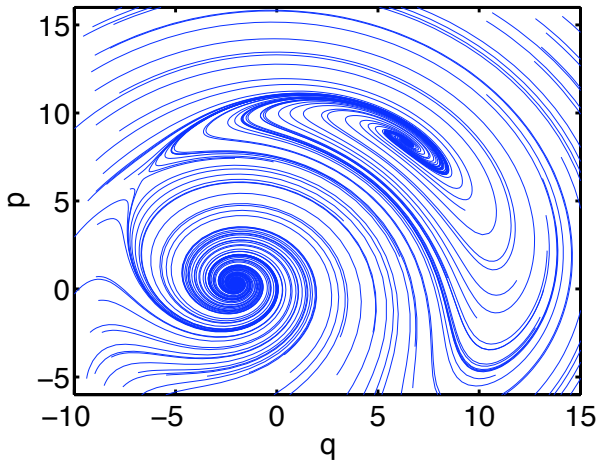

Figure 2. Phase space flow in the bistable regime for $\Delta\omega = -5$ (same parameters as in figure 1)

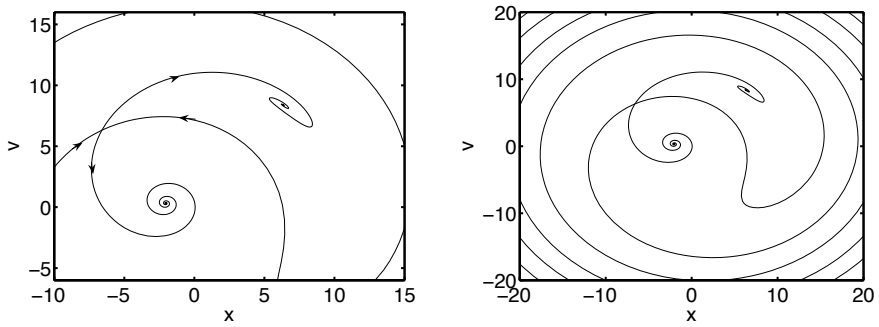

Figure 3. The stable manifolds of the unstable fixed point separate the basins of attraction of the two sinks.

Classical – quantum correspondence

In the following we will explore the classical – quantum correspondence. The quantum eigenvalues E_n, $n = 1,2,\ldots$, and eigenstates $|\phi_n\rangle$ of the non-Hermitian Hamiltonian $\hat{H} = \hat{H} - \mathrm{i}\hat{\Gamma}$, where $\hat{H}$ and $\hat{\Gamma}$ are given in (11) and (12), can be easily calculated numerically [8]. All calculations have been carried out for the same parameters used in the classical computations ($\kappa = 1.5$, $\beta = -7$ and $\chi = 0.05$) unless explicitly stated. The states are ordered with respect to their stability $\mathrm{Im}(E_n) > \mathrm{Im}(E_{n+1})$, i.e. state $n = 1$ is the most stable one.

Let us start our investigation of the quantum dynamics for parameters $\kappa = 1.5$, $\beta = -7$ and $\chi = 0.05$ and $\Delta\omega - 5$ already used in the classical phase space plots shown in figures 2 and 3.

The energy eigenvalues are shown in the complex energy plane (figure 4) and as a function of the index n (figure 5). We observe that the eigenvalues are clearly organized in three groups, labeled (a), (b) and (c), tracing out lines which show a pronounced crossing. In group (a) we find the most stable states and in group (c) the most unstable ones. In both groups, the imaginary¡ part of the energy varies rapidly with the state number. In group (b) this variation is much more modest. The real part for groups (a) and (b) decreases almost linearly with n, with the exception of the states $n = 26, 31, 52, 75$ whose real parts are almost equal. The real part in group (c) increases with n, starting from the value of the exceptional states.

Figure 6 shows the expectation values of position, $Q = \langle\hat{q}\rangle$, and momentum, $P = \langle\hat{P}\rangle$, as a function of the state number n as well as the uncertainty product. Again, there are marked differences for the three groups and the exceptional states.

The different character of the quantum eigenstates is elucidated in a plot the expectation values Q and P in phase space in figure 7. This again shows a localization of three lines with a crossing point. Also shown in the figure are the classical fixed points and the stable and unstable manifolds of the saddle point (compare figure 3). Obviously the three groups of states are organized by the classical fixed points. The most stable states in group (a) correspond to the most stable classical sink at $(q_1, p_1) = (-2.04, 0.32)$. This is also evident from the two examples of Husimi phase space distributions shown in figure 8 for states $n = 1$ and $n = 10$. Note that the quantum state $n = 1$ with maximum stability is localized at the classical fixed point. The uncertainty product for this state is equat to $\Delta x \delta p = 0.5001$, i.e. it

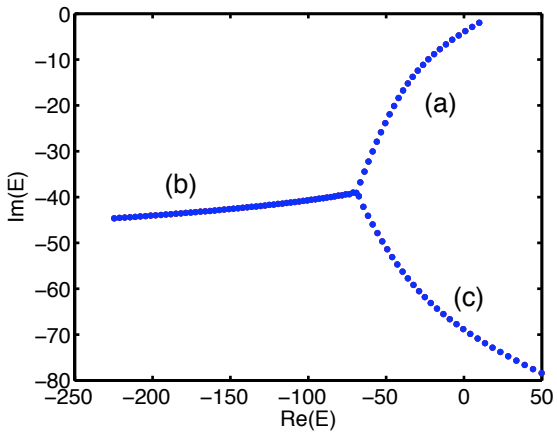

Figure 4. Complex energy eigenvalues

is almost a minimum uncertainty state. The other states of group (a) appear to be somewhat more extended in phase pace and localize at phase space points which follow a smooth line.

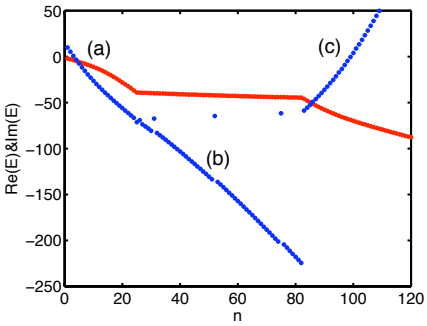

Figure 5. Energy eigenvalues real part (blue) imaginary part (red), $\langle Q \rangle$ (blue), $\langle P \rangle$ (red)

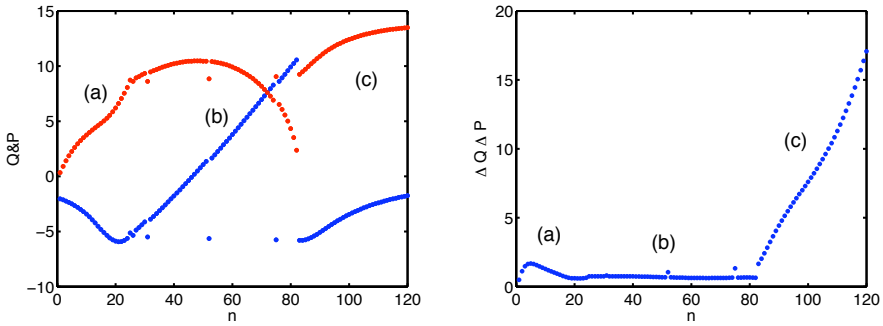

Figure 6. Left panel: Expectation values $\langle Q \rangle$ (blue), $\langle P \rangle$ (red) for the eigenstates as a function of the state number n. Right panel: Uncertainty product $\Delta q \Delta q$.

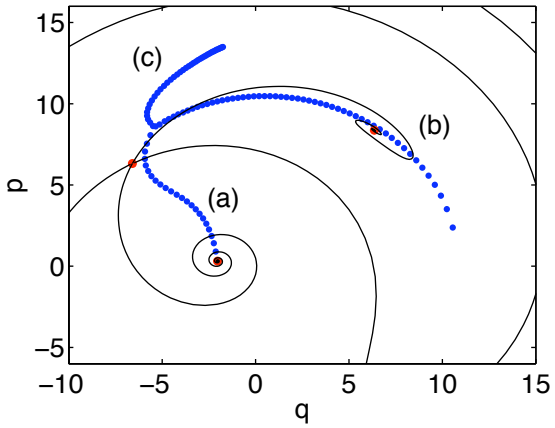

Figure 7. Expectation values $\langle Q \rangle$ $\langle P \rangle$ in phase space together with the classical stable and unstable manifolds of the unstable fixed points. The classical fixed points are shown as red dots.

xxx ich habe keine Idee, warum das so ist xxx

The states of group (b) show a different behavior. They are all of a similar size and their centers are located on a smooth line passing through (or close to) the classical fixed point $(q_2, p_2) = (6.36, 8.36)$. The rightmost of these points in figure 7, state $n = 82$, is the most unstable state of this group. Along the series of states towards the crossing point their stability increases. As an example, Husimi distributions are shown in figure 9 for $n = 82$ and $n = 60$.

The exceptional states all localize at the classical saddle point $(q_3, p_3) = (-6.59, 6.31)$. Their Husimi distributions are shown in figure 10.

Finally, the states of group (c) are very unstable and more extended in phase space, which is also seen from the uncertainty product in figure 6. Note that the number of states in this group depends on the numerics, i.e. on the number of states taken into account in the numerical matrix diagonalization.

The exceptional states clesrly show up in the overlap plots in figure 12.

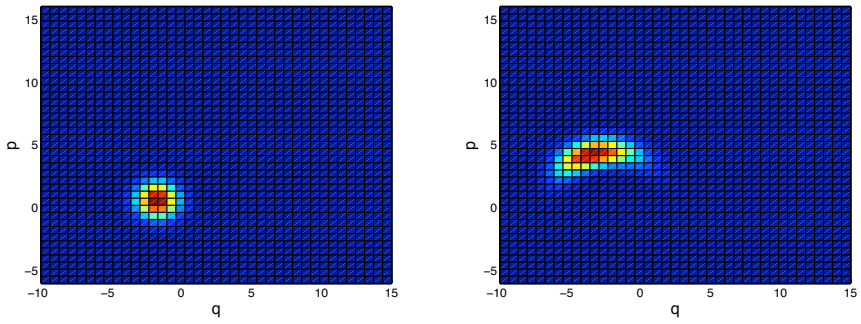

Figure 8. Husimi phase space distributions for states $n = 1$ and $n = 10$ of type (a).

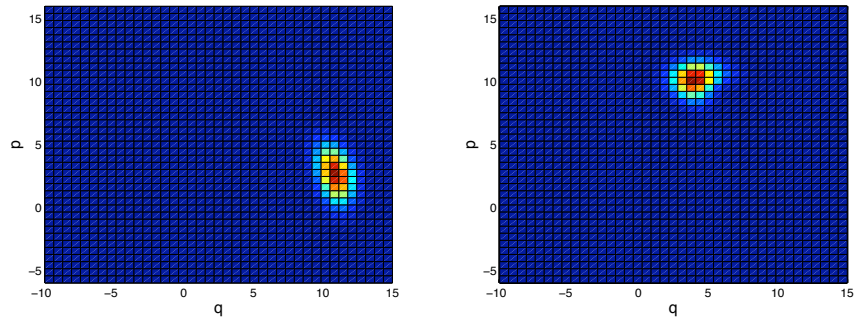

Figure 9. Husimi phase space distributions for states $n = 82$ and $n = 60$ of type (b).

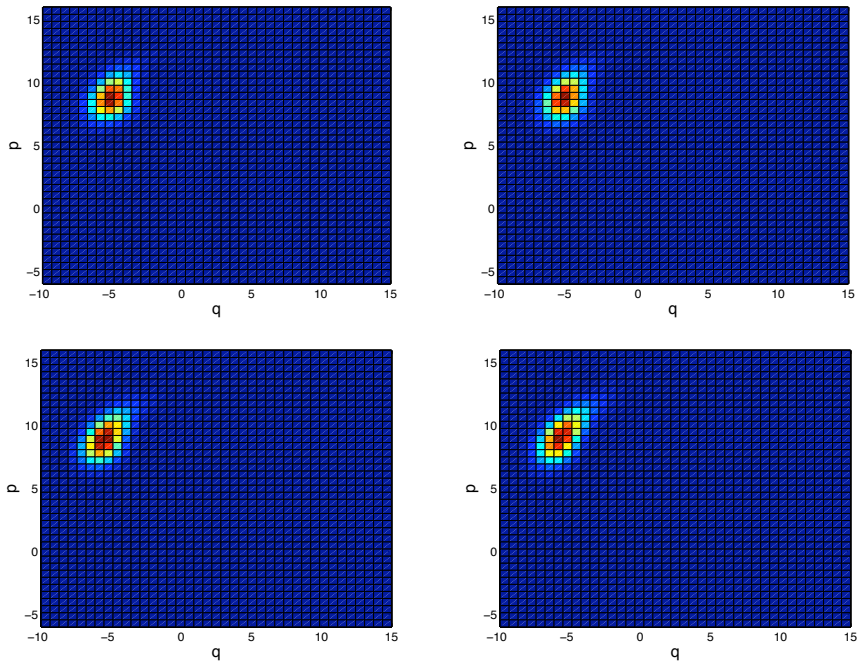

Figure 10. Husimi phase space distributions for states $n = 26, 31, 52, 75$ which are close to the bifurcation point of the different types of states (a), (b) and (c).

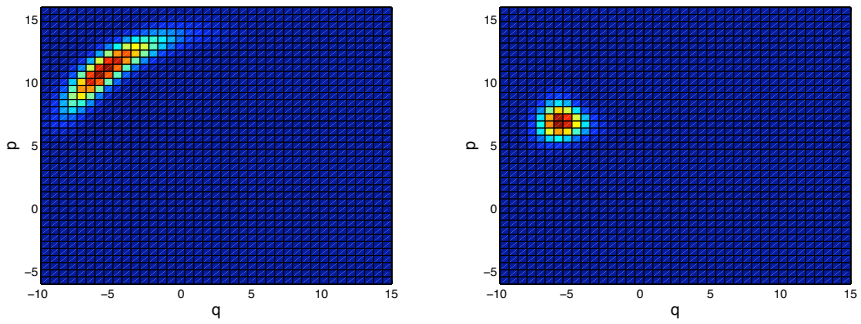

Figure 11. Husimi phase space distributions for state $n = 90$ of group (c) and for state $n = 21$ of group (a) which closest to the classical unstable fixed point (q_3, p_3).

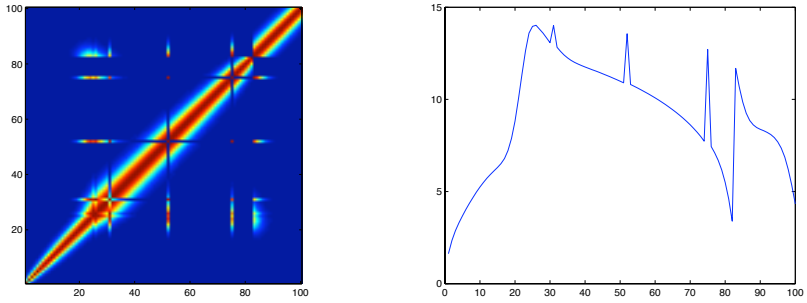

Figure 12. Overlap matrix of the different eigenstates (left) and the sum over its rows (right).

Exceptional points:

Petermann factor

$$K_n = \frac{\langle\tilde{\psi}_n|\tilde{\psi}_n\rangle\langle\psi_n|\psi_n\rangle}{|\langle\tilde{\psi}_n|\psi_n\rangle|^2} \tag{20}$$

where $|\psi_n\rangle$ are the eigenstates of $\hat{H}$ for eigenvalue E_n and $|\tilde{\psi}_n\rangle$ are the eigenstates of $\hat{H}^\dagger$ for eigenvalue E_n^*.

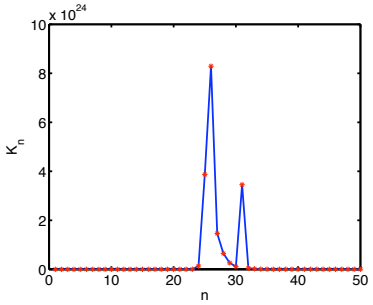

Figure 13. Petermann factor K_n for $\Delta\omega = -5$.

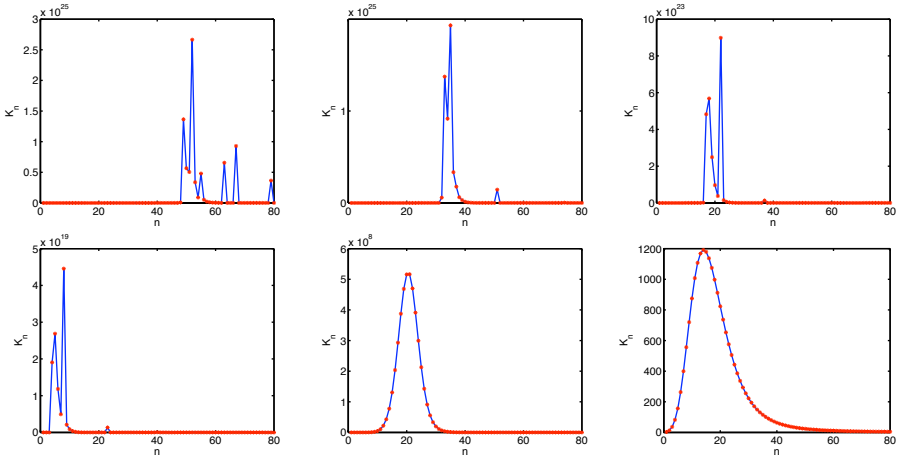

Figure 14. Petermann factor K_n for $Domega = -8, -6, -4, -2, 0$ and $+2$.

Quantum time evolution:
Following a numerical experiment in [7] using quantum state diffusion, we calculated the time dependence of $\langle\hat{q}\rangle$ and $\langle\hat{p}\rangle$ for an initially coherent state localized at $(q,p) = (7,14)$ for the non-Hermitian Hamiltonian (same parameters as above and in [7], figure 3). The resulting dynamics is shown in phase space in figure 15. This should be compared, of course, with figure 3 in [7], but also with the classical separatrices which are also shown in the figure. The position of the initial state (marked by a $*$ in the figure) is inside the basin pf attraction of the fixed point (q_2, p_2) therefore the quantum dynamics shows a tunneling process to the more stable one (q_1, p_1) by a separatrix crossing.

xxx irgenwie ist hier die Anfangsbedingung in de QM verschoben xxx
xxx besser qm und klassik in EIN bild xxx
xxx hier sollte man auch mal die Zeitabhängigeit von Q und P plotten! xxx

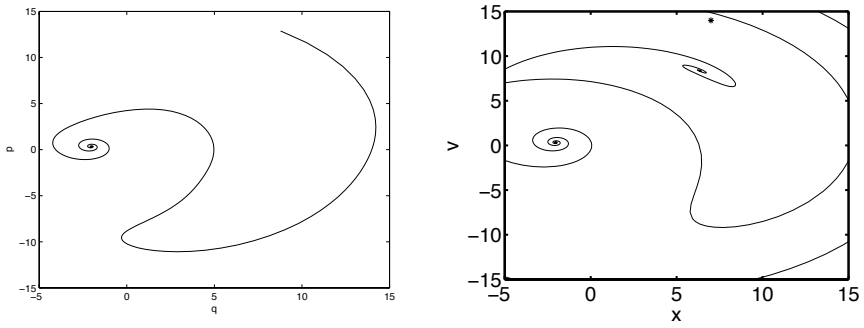

Figure 15. Left panel: Time evolution of $\langle\hat{q}\rangle$ and $\langle\hat{p}\rangle$ in phase space for an initial coherent state localized at $(q,p) = (7,14)$. [7], Fig.3, however for the non-Hermitian Hamiltonian. Right panel: Classical separatrices. The position of the initial state is marked by $*$.

Parameter dependence:
In the preceding calculations we fixed the parameters to the value $\Delta\omega = -5$, where we have three fixed points in the classical dynamics. We observed that the most stable fixed point localizes on the classical sink (q_1, p_1) in phase space. In figure 16 the parameter $\Delta\omega$ is varied over the interval shown in figure 1 and the real- and imaginary parts of the most stable eigenvalue of the hamiltonian is shown in comparison with the classical energies at the fixed points. We observe a surprisingly (?) correspondence with the most stable classical fixed point energies, except from the region $-3.5 < \Delta\omega < -1.4$.

The 60 most stable eigenvalues are shown in figure 17 as a function of $\Delta\omega$ together with the classical values of the energy H and the damping Γ (see (13)) at the fixed points. In figure 18 the most stable 120 states are displayed. It is obvious that the quantum eigenvalues 'feel' the classical region of bistability, where the eigenvalues are reorganized.

Alternatively one can compute the expectation value of the excitation number $\langle \hat{a}^\dagger \hat{a} \rangle$ or the mean position $\langle \hat{q} \rangle$ or momentum $\langle \hat{p} \rangle$ for the eigenstates. In figure 19 we compare the mean quantum excitation number for the 40 most stable eigenstates with the real valued classical stationary points $|\alpha|^2$ (see also figure 1 in [7]).

xxx Das Bild ist nicht sehr informativ(?) denn die Hauptstruktur kommt von den Bergkämmen, und die stammen einfach von der tatsache, dass ddort die Imaginärtaeile

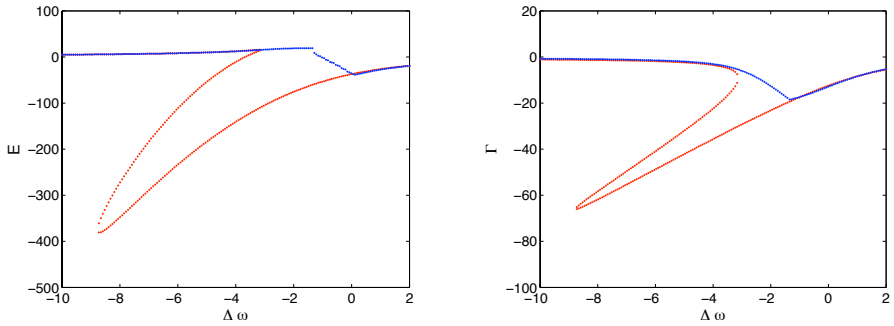

Figure 16. Real (left) and imaginary parts (right) of the most stable eigenvalues as a function of $\Delta\omega$ in comparison with the classical values of the energy H and damping Γ shown as red dots.(see (13)) at the fixed points. Parameters as in [7].

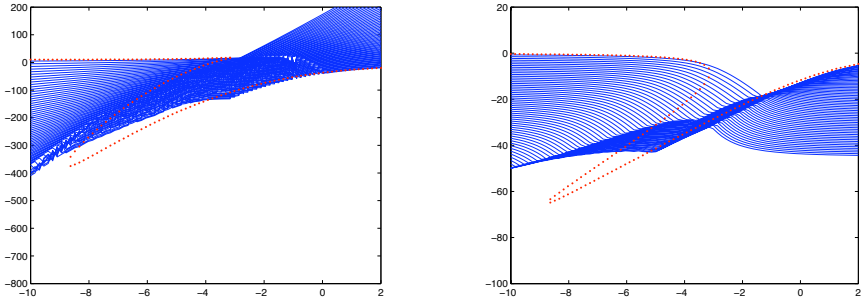

Figure 17. Real (left) and imaginary parts (right) of the 60 most stable eigenvalues as a function of $\Delta\omega$ in comparison with the classical values of the energy H and damping Γ shown as red dots.(see (13)) at the fixed points. Parameters as in [7].

kreuzen, dass also die Nummerierung der Zustände wechselt.

In order to explore the classical – quantum correspondence in the parameter regime where only a single classical fixed point exists, we repeat the calculations shown in figure 7 for parameters $\Delta\omega = -2$ (figure 20) and $\Delta\omega = 0$, $\Delta\omega = 2$ (figure 21). In the first case, the influence of the classical saddle point which disappeared into the complex extension of phase space, is still observable. Similar plots for $\Delta\omega = -10$ and $\Delta\omega = -12$ are shown in figure 22.

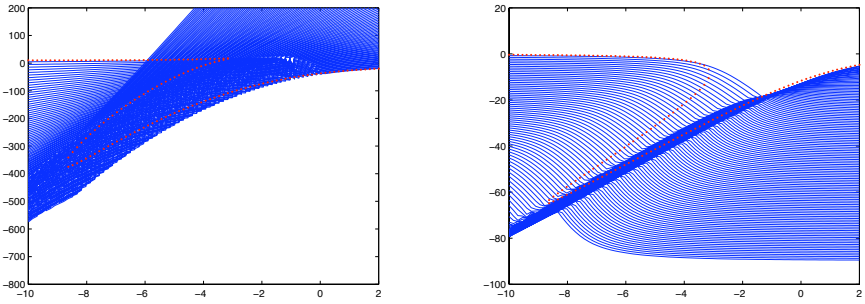

Figure 18. Real (left) and imaginary parts (right) of the 120 most stable eigenvalues as a function of $\Delta\omega$ in comparison with the classical values of the energy H and damping Γ shown as red dots.(see (13)) at the fixed points. Parameters as in [7].

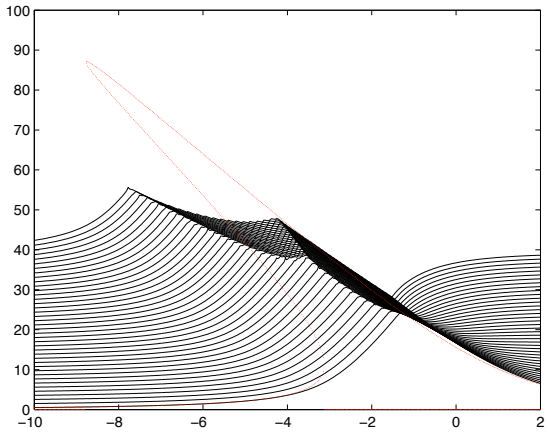

Figure 19. Expectation value of the excitation number $\langle \hat{a}^\dagger \hat{a} \rangle$ for the 40 most stable eigenstates in comparison with the real valued classical stationary points $|\alpha|^2$.

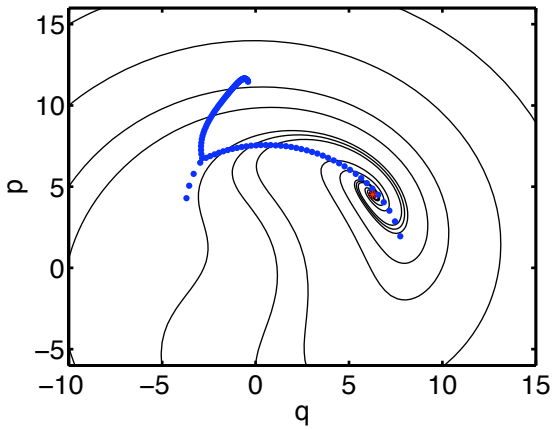

Figure 20. Expectation values $\langle Q\rangle$ $\langle P\rangle$ in phase space together with the classical stable and unstable manifolds of the unstable fixed points. The classical fixed points are shown as red dots. $\Delta\omega = -2$.

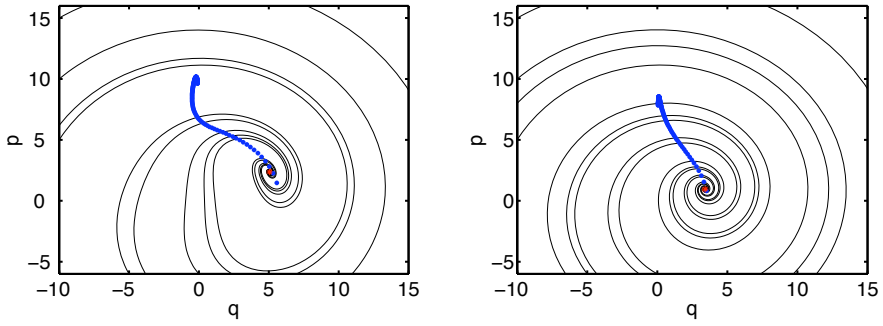

Figure 21. Expectation values $\langle Q\rangle$ $\langle P\rangle$ in phase space together with the classical stable and unstable manifolds of the unstable fixed points. The classical fixed points are shown as red dots. $\Delta\omega = 0$ (left) and $\Delta\omega = 2$ (right).

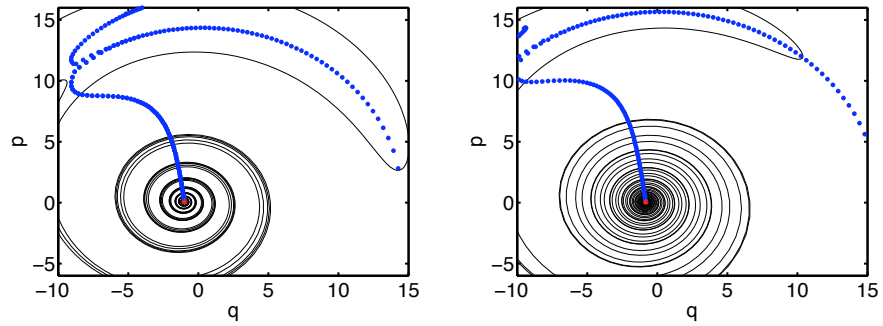

Figure 22. Expectation values $\langle Q\rangle$ $\langle P\rangle$ in phase space together with the classical stable and unstable manifolds of the unstable fixed points. The classical fixed points are shown as red dots. $\Delta\omega = -10$ (left) .

Acknowledgments

Support from the Deutsche Forschungsgemeinschaft via the Graduiertenkolleg "Nichtlineare Optik und Ultrakurzzeitphysik" is gratefully acknowledged.

References

[1] E. M. Graefe, M. Höning, and H. J. Korsch, J. Phys. A **43** (2010) 075306
[2] E. M. Graefe, H. J. Korsch, and A. E. Niederle, Phys. Rev. Lett. **101** (2008) 150408
[3] E.-M. Graefe, H. J. Korsch, and A. Niederle, Phys. Rev. A **82** (2010) 013629
[4] E.-M. Graefe and R. Schubert, arXiv:quant-ph/1010.4557 (2010)
[5] P. D. Drummond and D. F. Walls, J. Phys. A **13** (1980) 725
[6] D. Bortman and A. Ron, Phys. Rev. A **52** (1995) 3316
[7] M. Rigo, G. Alber, F. Mota-Furtado, and P. F. O'Mahony, PRA **55** (1997) 1665
[8] M. Glück and H. J. Korsch, Eur. J. Phys. **23** (2002) 413